Applied Surface Science 611 (2023) 155626

Contents lists available at ScienceDirect

Applied Surface Science

journal homepage: www.elsevier.com/locate/apsusc

Full Length Article

Simultaneously improved SERS sensitivity and thermal stability on Ag dendrites via surface protection by atomic layer deposition

Xinxin Wang [a,1], Lin Zhu [b,c,1], Zebin Zhu [a], Shaozhong Chang [b,c], Jisong Qian [a], Jianli Jiang [a], Xiaoxiong Wang [a], Aidong Li [b,c,*], Liyong Jiang [a,*], Yanqiang Cao [a,c,*]

[a] Institute of Micro-nano Photonics and Quantum Manipulation, School of Science, Nanjing University of Science and Technology, Nanjing 210094, China
[b] Materials Science and Engineering Department, College of Engineering and Applied Sciences, Collaborative Innovation Center of Advanced Microstructures, Nanjing University, Nanjing 210093, China
[c] Laboratory of Solid State Microstructures, Nanjing University, Nanjing 210093, China

ARTICLE INFO

Keywords:
Nanogaps
Ag dendrites
Atomic layer deposition
SERS
Stability

ABSTRACT

Silver has been considered as one of the most promising materials for surface-enhanced Raman scattering (SERS) thanks to its ultra-high sensitivity. Nevertheless, Ag based nanostructures suffer from both thermal and chemical instability, inhibiting their practical applications. Surface coating is effective for improving their stability, nevertheless, which sacrifices the SERS sensitivity. Here we proposed a novel strategy to fabricate highly sensitive and stable SERS substrates using atomic layer deposition (ALD) protected Ag nanogaps. The purpose of this work is to provide an ultrathin and conformal protective layer without destroying the hot spots in nanogaps. This idea was implemented in ALD protected Ag dendrites. Ultrathin ALD layer with precisely controlled thickness can be conformally coated on the Ag surface without blocking the nanogaps between adjacent branches. Experimental results revealed Ag dendrites@10-cycle ZnO exhibit the improved SERS sensitivity compared to the pristine Ag dendrites. COMSOL theoretical simulations also demonstrated that ultrathin ZnO coating can promote the plasmonic coupling in Ag nanogaps. More importantly, this SERS substrate also shows excellent thermal stability at high temperature of 200 °C. Therefore, both SERS sensitivity and thermal stability of Ag dendrites can be enhanced via ALD surface protection.

1. Introduction

Surface enhanced Raman scattering (SERS) technology can significantly amplify weak Raman signals with the characteristics of high sensitivity, molecular fingerprint recognition, rapid and non-destructive detection. Therefore, SERS has been widely used in biological detection, medical imaging, trace analysis, security and other fields [1–3]. SERS enhancement mechanism can be divided into electromagnetic enhancement and chemical enhancement. In most cases, electromagnetic enhancement is the main mechanism for SERS, which can cause a much higher enhancement factor than chemical enhancement. Usually, excellent electromagnetic enhancement can be achieved in noble metal (e.g. Au and Ag) nanostructures thanks to their unique localized surface plasmon resonance (LSPR) properties [4–6].

Ag has been considered as the most promising material for SERS due to its high electromagnetic enhancement effect and low cost (compared to Au). Therefore, tremendous efforts have been made to develop various Ag nanostructures for sensitive SERS substrates, such as nanoparticles, nanowires, nanocubes, nanorods, and dendrites [7–9]. Besides high sensitivity, stability is also a very important factor for practical applications. However, Ag nanostructures usually suffer from both structural and chemical instability. Ag surface can be oxidized or sulfured in air, moreover, the morphology of Ag nanostructures can't be maintained at high temperature. Both structural and chemical instability seriously dampen the sensitivity of Ag based SERS substrates [10]. Thus, it is important to improve the stability of Ag based SERS substrates for practical applications. Moreover, good thermal stability is essential for extending SERS's application at high temperature, such as *in situ* characterization of high temperature processes [10,11] and thermal annealing based self-cleaning [12].

It has been reported that surface coating is an effective strategy to enhance both structural and chemical stability of Ag nanostructures

* Corresponding author.
E-mail addresses: adli@nju.edu.cn (A. Li), jly@njust.edu.cn (L. Jiang), yqcao@njust.edu.cn (Y. Cao).
[1] These authors contributed equally to this work.

https://doi.org/10.1016/j.apsusc.2022.155626
Received 19 September 2022; Received in revised form 26 October 2022; Accepted 4 November 2022
Available online 8 November 2022

[10]. Among various surface modification methods, ALD has been proven to be the most promising technology due to its great 3D conformality, precise thickness control, and low deposition temperature [13,14]. ALD oxide coatings with nanometer scale have been demonstrated to elevate the stability of Ag based SERS substrates [12,15–18]. For example, Formo *et al.* protected the Ag nanowires with ~1.2 nm Al_2O_3, whose SERS sensitivity can be kept after annealing at 400 °C [15]. Ma *et al.* demonstrated that various ultrathin ALD oxides (Al_2O_3 [17], TiO_2 [18], HfO_2 [12]) can improve the stability of Ag nanorods. Although nanometer even sub-nanometer coating can be precisely prepared *via* ALD, the SERS sensitivity always decreases after surface coating. With the help of highly precise thickness control from ALD, Masango *et al.* reported a high-resolution distance-SERS study *via in-situ* SERS during ALD process, which demonstrated that SERS intensity of silver film on nanosphere (AgFON) would decrease even with only one cycle of ALD Al_2O_3 [19]. Therefore, it is still very challenging to stabilize the SERS substrates at high temperature *via* surface coating without sacrificing the SERS sensitivity.

Nanogaps based substrates were chosen for research here, where highly enhanced electromagnetic field can be obtained at the gap area [20–22]. If an ultrathin coating can cover the whole surface of Ag without blocking the gap area, reserving the hot spots in gap area, then both high sensitivity and stability may be achieved simultaneously. Various methods have been developed for fabricating metal nanogaps based SERS substrates in recent years, such as electron beam lithography and focused ion beam etching [23,24]. Although a variety of metal nanogap based SERS substrates with high sensitivity can be obtained, these microfabrication technologies suffer from high cost, high operation requirements, and low yield. The cost and large-scale fabrication must be taken into consideration for the practical applications of SERS substrates, too. Electrochemical deposition is a very facile, convenient, and cost-effective method to fabricate large area metal nanostructures, such as nanosheets [25], nanorods [26], nanowires [27], and dendrites [28]. Among them, metal dendrites have been demonstrated as the promising structures for SERS with plenty of branches and nanogaps, which can act as “hot spots” to generate high electromagnetic field [28–31]. For example, Zhao et al. reported that strong plasmon coupling formed in the nanogaps between adjacent branches of Ag dendrites. In addition, the enhancement increases with decreasing the gap size [28]. In this work, Ag dendrites prepared by electrochemical deposition were used as SERS substrates. The effect of ALD ZnO coating on the Raman sensitivity and thermal stability of Ag dendrites were investigated. The ZnO was chosen to construct semiconductor-metal junction with Ag, where surface plasmon resonance (SPR) can couple with electron transfer and trapping at defect states [32–34]. It was demonstrated that ultrathin ZnO layer (10 cycles, ~1.6 nm) can be conformally coated on the Ag surface without blocking the gap. As a result, both improved SERS sensitivity and thermal stability were achieved simultaneously.

2. Experimental section

2.1. Electrochemical deposition of Ag dendrites

The fabrication process of SERS substrates is illustrated in Fig. S1. Ag dendrites were first prepared in a two-electrode electrochemical deposition system using an electrochemical workstation (CHI660E). The ITO glass and silver plate were used as cathode and anode, respectively. $AgNO_3$ (0.01 M) and citric acid (0.2 M) mixture solution was employed as electrolyte. ITO glasses were ultrasonically cleaned in isopropanol, ethanol, and DI water for 5 min, respectively. The deposition current density and time were optimized to be 2 mA cm^{-2} and 180 s, respectively. After electrochemical deposition, Ag dendrites were rinsed with DI water and dried in air.

2.2. Synthesis of ZnO coated Ag dendrites

A home-made viscous-flow, hot-walled ALD reactor was utilized, where high purity N_2 (99.999%) was adopted as carrier and purging gas at a pressure of 0.9 Torr. The ZnO ALD process was conducted by alternating 2 s diethylzinc (DEZ, 6 N, Nanjing ai mou yuan Scientific equipment Co., Ltd.) and 2 s water dose, separated by 8 s N_2 purging. The thickness of ZnO was controlled by the ALD deposition cycles (5–50). Both DEZ and water were at room temperature. A low deposition temperature of 80 °C was chosen for ALD process to avoid damage to Ag dendrites.

2.3. Characterizations

Crystallinity and phase structures were measured by X-ray diffraction (XRD, XD6, Beijing Pgeneral) with Cu Kα radiation. Surface chemical information was detected using X-ray photoelectron spectroscopy (XPS, Thermo Fisher K-Alpha) with standard Al Kα (1486.7 eV) X-ray source, where the binding energy of C1*s* (284.6 eV) was used for calibration. Microstructures and morphology were observed by both field emission scanning electron microscopy (FESEM, Ultra 55, ZEISS) and transmission electron microscopy (TEM, FEI Tecnai F20 S-Twin). Reflectivity was measured by a UV-NIR spectrometer (SR-303-iA, Andor).

2.4. SERS test

SERS substrates were first immersed into the 10^{-4} M methylene blue (MB) solution for 3 h. Then the substrates were rinsed with DI water and blown dry by N_2. A confocal Raman microscope (B&W TEK) was adopted for collecting Raman spectra of MB, whose excitation laser wavelength is 532 nm. The beam spot of laser was focused to be ~5 μm in diameter with the power of 0.4 mW. The collection time of each spectrum was set as 500 ms. 10 spectra were collected for each sample to measure and average the signals. For limit detection measurement, 10^{-3} M rhodamine 6G (R6G) solution was prepared, then various R6G (10^{-4}-10^{-10} M) can be obtained by diluting above solution. For thermal stability test, all the samples were heated in air for 30 min at various temperatures (100, 150, and 200 °C).

2.5. COMSOL simulation

Simulation of the electric field enhancement was performed by the commercial software COMSOL Multiphysics based on the finite element method (FEM). The structural parameters of Ag dendrites for modeling were set according to the size measured from SEM/TEM images, and the complex refractive indices of Ag and ZnO were fitted to experimental dates [35,36]. A typical discretization of Ag dendrites is given in Fig. S2. In the frequency-domain calculation, the perfectly matched layers (PML) were applied in the x and z directions and the periodic condition was applied in the y direction. A plane wave polarized in the x direction was incident to the structure along -z direction to excite the surface plasmons.

3. Results and discussions

The composition and microstructures of Ag dendrites prepared at 2 mA cm^{-2} for 180 s were first characterized. Fig. 1(a) presents the XPS spectrum of Ag 3d, exhibiting the doublet of Ag $3d_{5/2}$ and Ag $3d_{3/2}$ at 368.4 and 374.4 eV. It implies that Ag dendrites are at metallic state. Fig. 1(b) displays the XRD pattern of Ag dendrites. Besides the signal from substrate of ITO, four diffraction peaks at 38.1, 44.4, 64.5, and 77.5° correspond to the (111), (200), (220), and (311) crystal planes of Ag structure (JCPDS No. 04-0783) can be observed, indicating Ag dendrites are well crystallized. Moreover, intensity from (111) plane is much higher than other planes, indicating that Ag dendrites grow

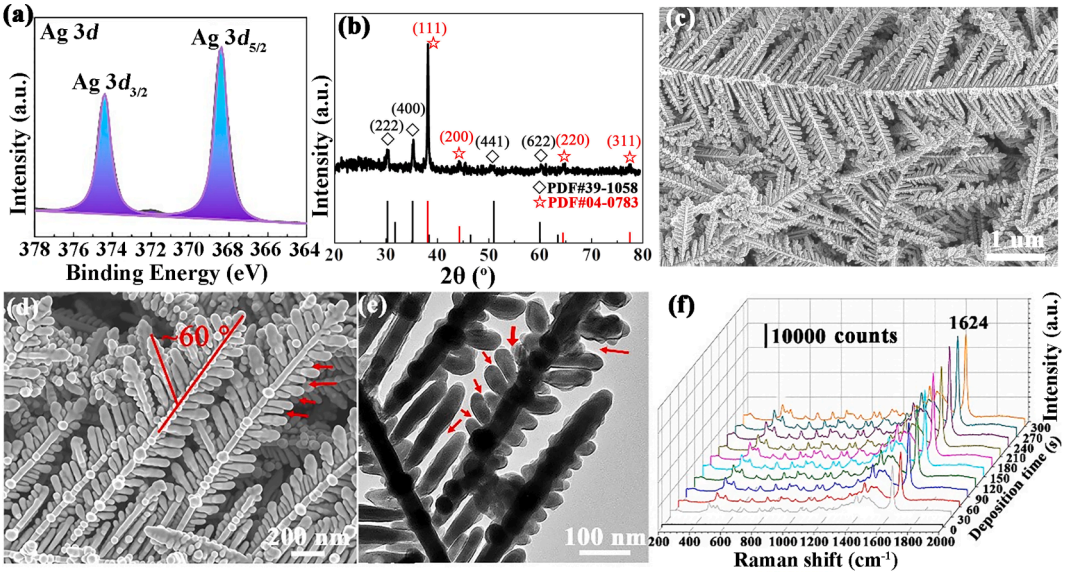

Fig. 1. (a) XPS spectrum of Ag 3d and (b) XRD pattern of the as deposited Ag dendrites. (c,d) SEM and (e) TEM images of Ag dendrites obtained at 2 mA cm^{-2} for 180 s. (f) SERS spectra of 10^{-4} M MB on Ag dendrites with various deposition time from 30 to 300 s.

preferentially along in the direction of {1 1 1} crystal plane. The typical morphology of Ag dendrites prepared by electrochemical deposition was characterized by SEM and TEM, as presented in Fig. 1(c-e). Highly branched dendrites were formed on the whole substrate, where each Ag dendrite is consisted of the central long backbone and many side branches, similar with previous literatures [28–31]. Further observation shows that the angles between backbone and branches are nearly the same (~60°), as identified in Fig. 1(d), also implying that Ag dendrites grow preferentially/selectively in the definite direction. Therefore, the obtained the silver nanostructures can possess plenty of branches and nanogaps, which can act as "hot spots" to generate high electromagnetic field.

The parameters of current density and deposition time were optimized to be 2 mA cm^{-2} and 180 s, respectively, as shown in Fig. S3 and Fig. 1(f). The ITO glass shows no SERS activity, a high Raman signal can be detected after a short deposition time of 30 s. But only few short dendrites can be observed with some flower-like nanoparticles scattered on the ITO surface for short deposition time, as shown in Fig. S4(a). When the deposition time is extended to be 180 s, the Ag dendrites grow longer and more complicated with plenty of branches on the whole substrate (Fig. 1c,d). Further prolonging the deposition time to be 300 s, similar multi-level branched Ag dendrites were obtained, as displayed in Fig. S4(b). As a result, Raman intensity increases with extending the deposition time first, then it keeps nearly unchanged when deposition time is between 180 and 300 s, as displayed in Fig. 1(f) and S3(b).

Then various cycles of ALD ZnO were coated on Ag dendrites, and the effect of ALD ZnO coating on the SERS sensitivity was first explored. The samples were marked as Ag D@x-cycle ZnO, where x refers to the ALD cycle number. Interestingly, the Raman intensity increases first then decreases with increasing the cycles of ALD ZnO coating, where 10 cycles ZnO coated Ag dendrites exhibit the highest SERS sensitivity. While 50 cycles ZnO coated Ag dendrites show nearly no SERS activity, therefore, whose Raman spectra was presented at 10 times magnification for comparison here, as shown in Fig. 2. The above phenomenon is quite different from previous literatures, where the SERS sensitivity always decreases after ALD coating, as presented in Table 1.

The microstructures and composition of ZnO coated Ag dendrites were characterized, as shown in Fig. 3 and S5. Fig. 3(a) shows the morphology of Ag D@10-cycle ZnO, it can be seen that there is no obvious change compared to as prepared Ag dendrites. The Ag nanogaps still exist after being coated with such an ultrathin ZnO. The corresponding elemental mapping using EDX was conducted for Ag and Zn, as

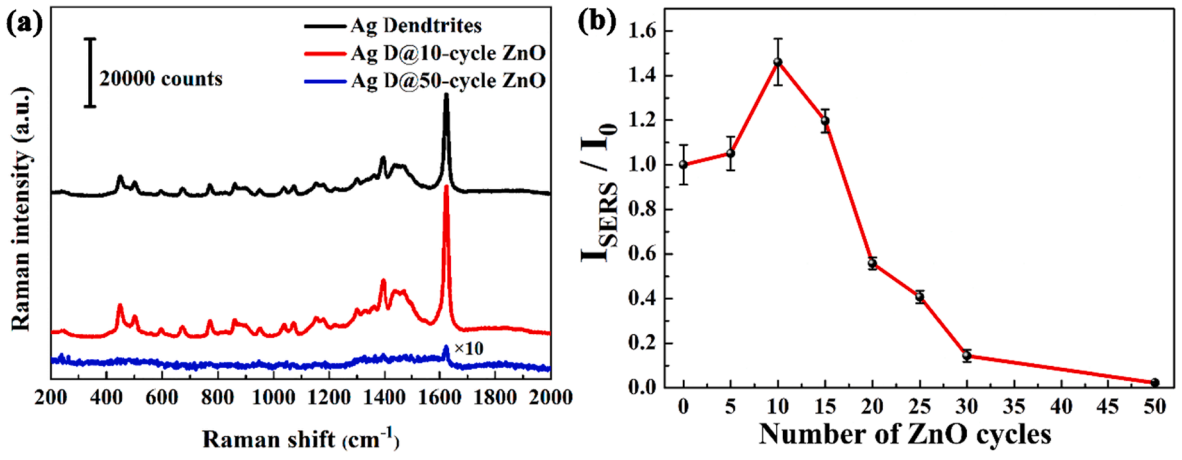

Fig. 2. (a) Raman spectra of 10^{-4} M MB on Ag dendrites, Ag D@10-cycle ZnO and Ag D@50-cycle ZnO. (b) Normalized Raman intensity at 1624 cm^{-1} versus the cycles of ALD ZnO coating, where I_0 refers to the intensity of pristine Ag dendrites.

Table 1
Comparation of ALD coated Ag nanostructures for SERS.

SERS substrates	ALD coating /thickness(nm)	Target	Raman signal reservation (%)*	Ref
Ag nanowires	Al_2O_3/1.2	R6G	68	[15]
Ag island film	Al_2O_3/2.5	R6G	42	[16]
	Al_2O_3/5	R6G	22	[16]
	TiO_2/3	R6G	4.3	[37]
Ag nanorod	Al_2O_3/1.5	MB	45	[17]
	TiO_2/1.65	CV	43	[18]
AgFON	Al_2O_3/0.7	TMA	20	[19]
	Al_2O_3/3	TMA	7	[19]
Ag dendrites	ZnO/1.6	MB	146	This work

* Note: Raman signal reservation (%) is determined by the ratio of Raman intensity after ALD coating to pristine SERS substrate.

shown in Fig. 3(b)(c). It is revealed that ZnO is coated on the whole branches of Ag dendrites. XPS spectra in Fig. S5 can detect both Ag and Zn, also confirming the formation of ultrathin ZnO on Ag surface. TEM was further performed to characterize the micro morphology of Ag D@10-cycle ZnO, as shown in Fig. 3(d). It can be seen that the whole surface of Ag dendrites is uniformly coated with an ultrathin ZnO of ~1.6 nm. It should be noted that the nanogaps are not blocked after ALD coating due to its excellent conformality, as marked in Fig. 3(d). Fig. 3(e) presents the morphology of Ag dendrites after a thick ZnO coating with 50 cycles. The silver branches become bigger and are close to each other. TEM image in Fig. 3(f) can more clearly show the morphology of Ag D@50-cycle ZnO. ~8 nm ZnO is observed on the tips of Ag dendrites, while the gap areas are filled with ZnO. The hot spots area in nanogaps are lost, therefore, Ag D@50-cycles ZnO exhibits nearly no SERS activity.

Based on SEM and TEM, it can be seen that nanogaps can be maintained after ultrathin ZnO coating (~1.6 nm), resulting in high SERS sensitivity. In order to further explore the mechanism for the improvement of SERS sensitivity after ultrathin ZnO coating (5–15 cycles), theoretical simulations were conducted using the commercial software COMSOL Multiphysics based on the finite element method (FEM). Fig. 4 (a)(b) illustrates the field distribution in pristine Ag dendrites, it can be found that enhanced electric field locates at the tips of Ag branches and the nanogap area between adjacent Ag branches, indicating strong plasmonic coupling formed in nanogaps. Then, various thickness of ZnO (0.8–8 nm or 5–50 ALD cycles) coating were introduced into the Ag dendritic structures, whose calculated electrical field distributions are displayed in Fig. 4(c-h). Similarly, most of enhanced electrical field locates at the nanogaps, moreover, the electrical field in air is much larger than that in ZnO. More interestingly, it can be found that the electrical field in air area of nanogaps increases with increasing the thickness of ZnO layer before blocking the nanogaps, as plotted in Fig. 4(i). The absorptance spectra of Ag dendrites with various ZnO coating were also calculated, as shown in Fig. S6. It can be seen that the absorption peak of

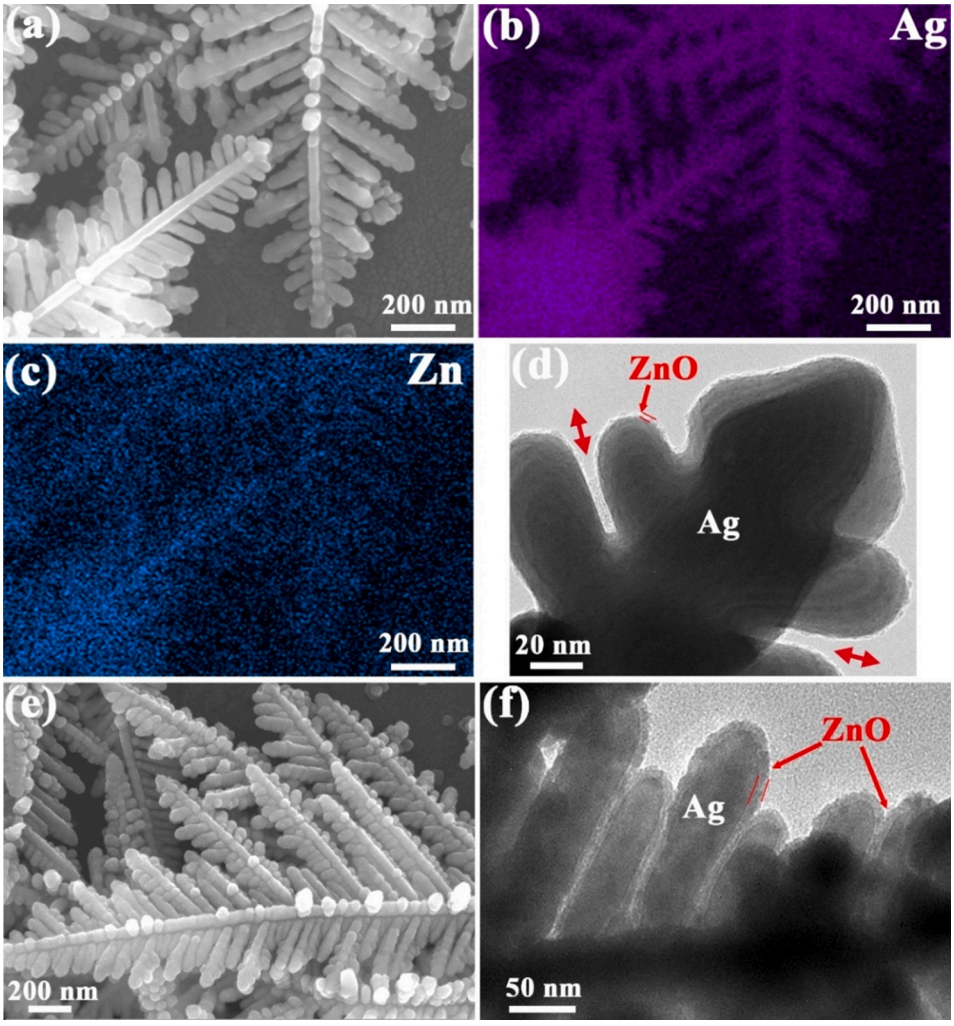

Fig. 3. (a) SEM image of Ag D@10-cycle ZnO. The corresponding EDX elemental distribution of (b) Ag and (c) Zn. (d) TEM image of Ag D@10-cycle ZnO. (e) SEM and (f) TEM images of Ag D@50-cycle ZnO.

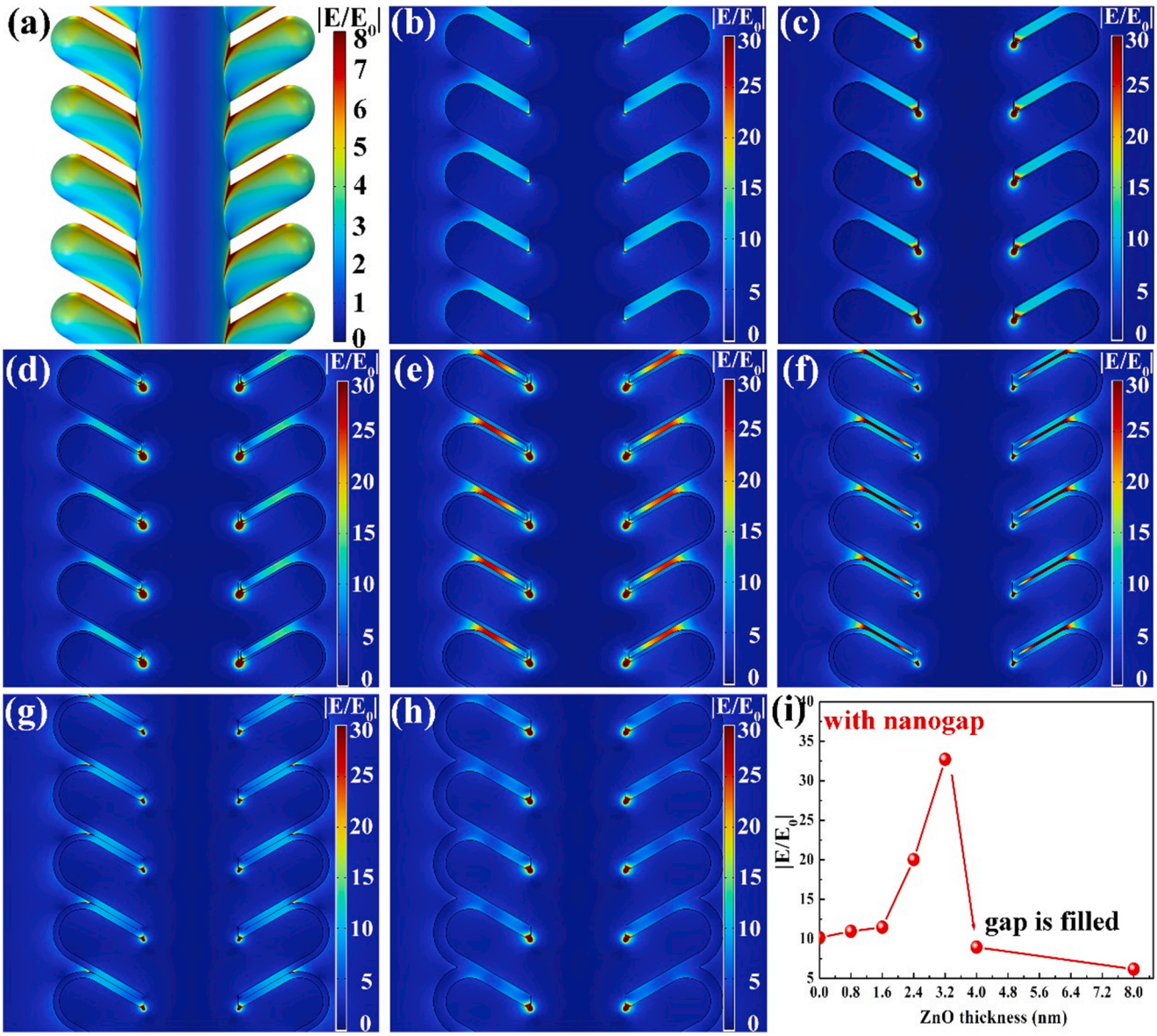

Fig. 4. COMSOL simulations of local field distribution at excitation laser wavelength of 532 nm for Ag dendrites (8 nm gap) with various thickness of ALD ZnO coating: (a) (b) 0, (c) 0.8, (d) 1.6, (e) 2.4, (f) 3.2, (g) 4.0, (h) 8.0 nm. (i) Local field intensity at the gap versus the thickness of ALD ZnO.

pristine Ag dendrites (8 nm gap size) locates at ~502 nm, which red-shifts after ZnO coating. The absorption peak of Ag D@ZnO gets closer and closer to the excitation wavelength of 532 nm in the COMSOL simulation. Therefore, ultrathin ZnO coating on Ag dendrites can tune the plasmonic coupling in Ag nanogaps. When the nanogaps are filled with ZnO, the Ag dendrites lose their hotspots. The electrical field exposed is much weaker than that in other structures with nanogaps.

ZnO can not only tune the plasmonic coupling in Ag nanogaps, but also construct the semiconductor-metal junction with Ag. The band alignment of ZnO-Ag is shown in Fig. S7. The conduction band (CB) of ZnO is located at −4.19 eV vs. absolute vacuum scale (AVS), and the Fermi level of silver is at −4.26 eV vs. AVS [32]. The SPR generated electrons of Ag can easily transfer to CB of ZnO, as illustrated in Fig. S7. Secondly, Edri et al. recently reported that defects (Ag-O-Zn bonds and oxygen vacancies) at ZnO/Ag interface can also act as electronically active traps [33]. Therefore, SPR couples with electron transfer and trapping in Ag-ZnO nanostructures, which can prevent the recombination of SPR electron-hole pairs, thus a significant improvement of SERS properties can be anticipated [34].

Based on above experiments and theoretical simulations, it can be demonstrated that ultrathin ZnO coating in Ag nanogaps can promote the plasmonic coupling between adjacent Ag branches, enhancing the SERS sensitivity. However, when nanogaps are filled with ZnO, the SERS sensitivity would be very weak due to losing their main hotspots. The gap size of in Ag dendrites is not uniform, smaller nanogaps will be more easily filled. More and more nanogaps would be filled with ZnO along with increasing the thickness of ALD coating. In addition, the size of MB molecule is ~1.70 nm × 0.76 nm × 0.325 nm, it may be more and more difficult to enter the nanogap area with decreasing the gap size. As a result, it can be observed in experiments that Ag dendrites with 10 cycles ZnO exhibits the best SERS sensitivity.

Besides sensitivity, stability of SERS substrates is also very important for practical applications. Both Ag dendrites and Ag D@10-cycle ZnO are stable in air at room temperature, as shown in Fig. S8. However, pristine Ag dendrites exhibit poor thermal stability, whose Raman intensity degrades dramatically after 30 min heating in air at 150 and 200 °C, as displayed in Fig. 5(a). While Ag D@10-cycle ZnO shows excellent thermal stability even after 30 min heating in air at high temperature of 200 °C, as shown in Fig. 5(b). In order to investigate the degradation mechanism of Ag dendrites after heating, composition and

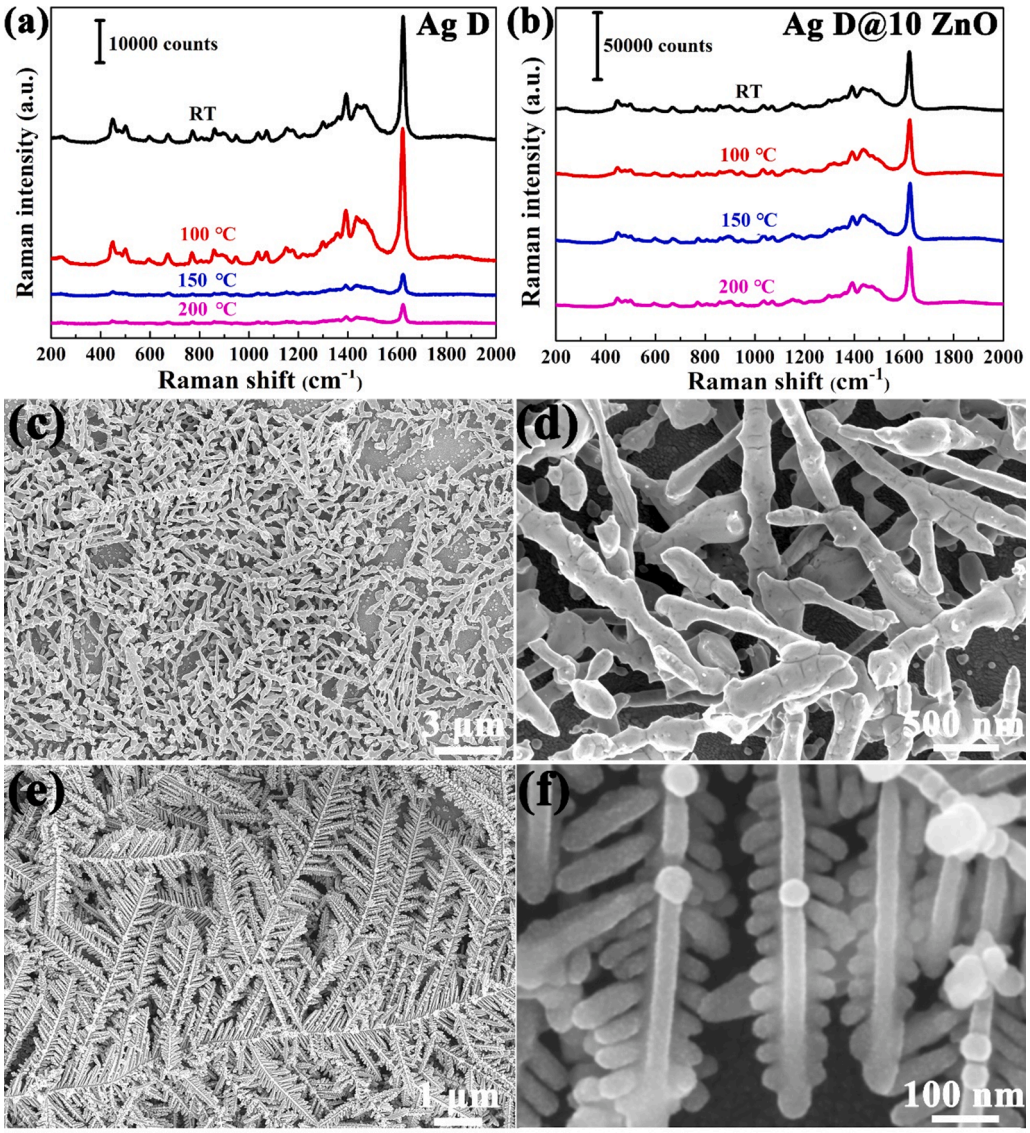

Fig. 5. Raman spectra of MB on (a) pristine Ag dendrites and (b) Ag D@10-cycle ZnO before and after annealing at 100, 150, and 200 °C, respectively. SEM images of (c)(d) pristine Ag dendrites and (e)(f) Ag D@10-cycle ZnO after annealing at 200 °C.

microstructures were characterized. Both XRD and XPS results indicate that Ag still stays at metallic state after 200 °C heating, as shown in Fig. S9 and S10, which is consistent with previous reports [38]. However, the sample's color turned into white from grey after heating, then, the reflectivity of the samples was characterized before and after heating, as illustrated in Fig. S11. The reflectivity of pristine Ag dendrites increases after heating, while Ag D@10-cycle ZnO exhibits the stable reflectivity spectra.

Then, the morphology change after heating was explored. The morphology of pristine Ag dendrites exhibits great change after 200 °C heating, only leaving coarse branch without nanogaps, as shown in Fig. 5(c)(d). Therefore, the morphological instability of Ag dendrites may be the main factor leading to their SERS fading at high temperature. On the contrast, 10 cycles (~1.6 nm) ZnO coated Ag dendrites show excellent thermal stability, whose morphology with plenty of nanogaps can be maintained, as shown in Fig. 5(e)(f). The corresponding EDX mapping of Ag and Zn was shown in Fig. S12. Thus, it can be demonstrated that an ultrathin ZnO can stabilize the morphology of Ag dendritic nanostructures at high temperature, then maintaining the SERS sensitivity.

Except for sensitivity and stability, reproducibility is another important issue for SERS substrates. To test the reproducibility, SERS spectra of MB were recorded at 20 random spots on Ag D@10-cycle ZnO after 200 °C heating, as displayed in Fig. S13(a). The corresponding relative intensity variation (@1624 cm^{-1}) was plotted in Fig. S13(b), exhibiting the relative standard deviation (RSD) of 9.0%. This result indicates ZnO coated Ag dendrites can exhibit good reproducibility.

Besides, Ag dendrites or Ag D@10-cycle ZnO are capable of full spectrum absorption in visible range, as presented in Fig. S11. This is because that Ag dendrites are consisted of branches with various length and width, containing various nanogap sizes. Different scale morphology can result in a different resonance position, therefore, any excitation wavelength laser in visible range can match a plasmon resonance for Ag dendrites [36,37]. Therefore, a different excitation wavelength laser can be used here for SERS measurement. Fig. S15 shows the Raman spectra of MB obtained using 785 nm laser, as expected, excellent SERS performance can be observed.

To further illustrate the practicability of Ag D@ZnO based SERS substrates, rhodamine 6G (R6G), one of the most frequently used dyes, with various concentration (10^{-4}-10^{-10} M) were detected. It can be seen that characteristic peaks of R6G molecules can be also well detected. Fig. 6(a) displays the corresponding Raman spectra, the intensity

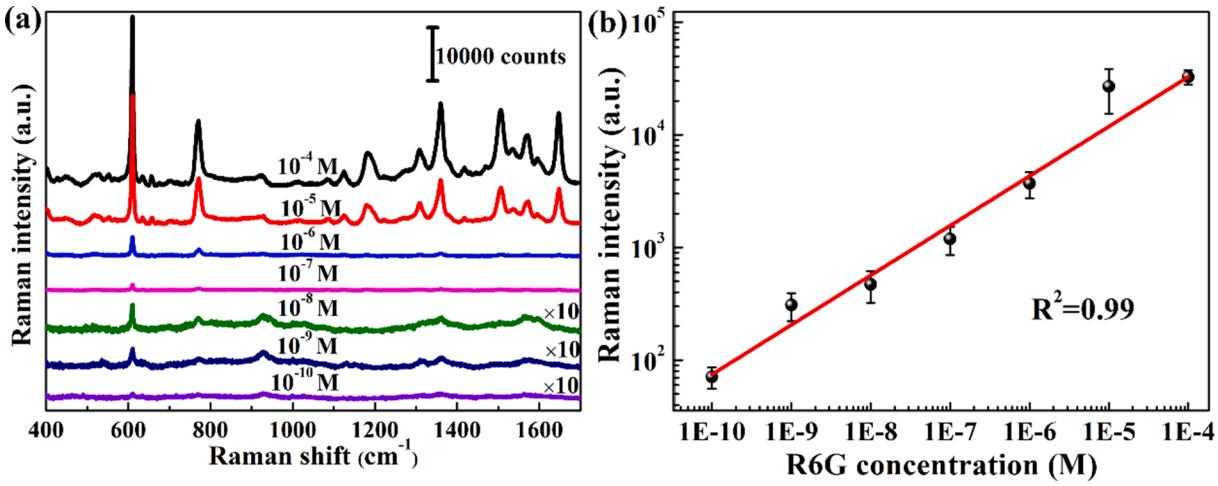

Fig. 6. (a) Raman spectra of R6G (10^{-4}-10^{-10} M) on Ag D@10-cycle ZnO, (b) the corresponding intensity (@610 cm^{-1}) versus the concentration of R6G.

decreases with decreasing the concentration of R6G. Ag D@10-cycle ZnO exhibits the detection limit of 10^{-10} M for R6G, where the main characteristic peaks can still be detected (Fig. S16). In addition, the intensity (610 cm^{-1}) versus the concentration was also plotted in Fig. 6(b), suggesting a nice linear relationship with correlation coefficient value (R^2) of 0.990. It implies Ag D@ZnO based SERS substrates show great prospects in nanomolar detection. Analytic enhancement factor (AEF) was applied to evaluate the performance using the equation of AEF= $(I_{SERS}/c_{SERS})/(I_{Raman}/c_{Raman})$ [39,40]. I_{SERS} and I_{Raman} are the intensity (@610 cm^{-1}) obtained on Ag D@10-cycle ZnO and Au film, which can be obtained from Fig. S16. c_{SERS} and c_{Raman} are the concentration of R6G under SERS and normal Raman conditions, which are 0.01 M and 10^{-10} M, respectively. Therefore, the AEF here is estimated to be $\sim 1.4 \times 10^{10}$.

4. Conclusions

In summary, Ag dendrites@ZnO based SERS substrates were prepared by the combination of electrochemical deposition and ALD modification. Both experimental results and theoretical simulations demonstrated that an ultrathin ZnO coating in Ag nanogaps can promote the plasmonic coupling, improving the SERS sensitivity. At the same time, SPR can couple with electron transfer and trapping in Ag-ZnO junctions. More importantly, ZnO coating can stabilize the nanostructures of Ag dendrites at high temperature of 200 °C. Therefore, both enhanced SERS sensitivity and improved thermal stability can be simultaneously achieved on Ag dendrites with ultrathin ALD coating. Ag D@10-cycle ZnO exhibits the detection limit of 10^{-10} M for R6G with a high AEF of 1.4×10^{10}. Results presented here demonstrate that it is a promising strategy to fabricate highly sensitive and stable SERS substrates by the combination of ALD and metal nanogaps, bringing SERS technology into practical applications.

CRediT authorship contribution statement

Xinxin Wang: Investigation, Methodology, Writing – original draft. **Lin Zhu:** Investigation, Methodology. **Zebin Zhu:** Validation. **Shaozhong Chang:** Investigation. **Jisong Qian:** Investigation. **Jianli Jiang:** Formal analysis. **Xiaoxiong Wang:** Validation, Formal analysis. **Aidong Li:** Formal analysis, Writing – review & editing. **Liyong Jiang:** Formal analysis, Writing – review & editing. **Yanqiang Cao:** Supervision, Conceptualization, Writing – review & editing.

Declaration of Competing Interest

The authors declare that they have no known competing financial interests or personal relationships that could have appeared to influence the work reported in this paper.

Data availability

Data will be made available on request.

Acknowledgements

This work was supported in part by the Natural Science Foundation of China (51802150, 61675096), open project from Laboratory of Solid State Microstructures (M33029), and Postgraduate Research & Practice Innovation Program of Jiangsu Province (KYCX22_0397).

Appendix A. Supplementary data

Supplementary data to this article can be found online at https://doi.org/10.1016/j.apsusc.2022.155626.

References

[1] X.X. Han, R.S. Rodriguez, C.L. Haynes, Y. Ozaki, B. Zhao, Surface-enhanced Raman spectroscopy, Nat. Rev. Methods Primers 1 (2022) 1–17.
[2] C. Zong, M. Xu, L.-J. Xu, T. Wei, X. Ma, X.-S. Zheng, R. Hu, B. Ren, Surface-Enhanced Raman Spectroscopy for Bioanalysis: Reliability and Challenges, Chem. Rev. 118 (2018) 4946–4980.
[3] R. Panneerselvam, G.-K. Liu, Y.-H. Wang, J.-Y. Liu, S.-Y. Ding, J.-F. Li, D.-Y. Wu, Z.-Q. Tian, Surface-enhanced Raman spectroscopy: bottlenecks and future directions, Chem. Commun. 54 (2018) 10–25.
[4] L.-L. Tan, M. Wei, L. Shang, Y.-W. Yang, Cucurbiturils-Mediated Noble Metal Nanoparticles for Applications in Sensing, SERS, Theranostics, and Catalysis, Adv. Funct. Mater. 31 (2021) 2007277.
[5] H. Kang, J.T. Buchman, R.S. Rodriguez, H.L. Ring, J. He, K.C. Bantz, C.L. Haynes, Stabilization of Silver and Gold Nanoparticles: Preservation and Improvement of Plasmonic Functionalities, Chem. Rev. 119 (2019) 664–699.
[6] X. Yang, Y. Liu, S.H. Lam, J. Wang, S. Wen, C. Yam, L. Shao, J. Wang, Site-Selective Deposition of Metal-Organic Frameworks on Gold Nanobipyramids for Surface-Enhanced Raman Scattering, Nano Lett. 21 (2021) 8205–8212.
[7] X. Xiu, L. Hou, J. Yu, S. Jiang, C. Li, X. Zhao, Q. Peng, S. Qiu, C. Zhang, B. Man, Z. Li, Manipulating the surface-enhanced Raman spectroscopy (SERS) activity and plasmon-driven catalytic efficiency by the control of Ag NP/graphene layers under optical excitation, Nanophotonics 10 (2021) 1529–1540.
[8] L. Li, W.S. Chin, Rapid Fabrication of a Flexible and Transparent Ag Nanocubes@PDMS Film as a SERS Substrate with High Performance, ACS Appl. Mater. Interfaces 12 (2020) 37538–37548.
[9] A. Loiseau, V. Asila, G. Boitel-Aullen, M. Lam, M. Salmain, S. Boujday, Silver-Based Plasmonic Nanoparticles for and Their Use in Biosensing, Biosensors 9 (2019) 78.
[10] Y. Liu, J. Lu, Y. Tao, N. Li, M. Yang, J. Shao, Ag-Embedded Silica Core-Shell Nanospheres for Operando Surface Enhanced Raman Spectroscopy of High-Temperature Processes, Anal. Chem. 92 (2020) 9566–9573.
[11] R.A. Hackler, G. Kang, G.C. Schatz, P.C. Stair, R.P. Van Duyne, Analysis of TiO_2 Atomic Layer Deposition Surface Chemistry and Evidence of Propene

Oligomerization Using Surface-Enhanced Raman Spectroscopy, J. Am. Chem. Soc. 141 (2019) 414–422.
[12] L. Ma, H. Wu, Y. Huang, S. Zou, J. Li, Z. Zhang, High-performance real-time SERS detection with recyclable Ag nanorods@ HfO_2 substrates, ACS Appl. Mater. Interfaces 8 (2016) 27162–27168.
[13] Y. Cao, X. Meng, A. Li, Atomic Layer Deposition of High-Capacity Anodes for Next-Generation Lithium-Ion Batteries and Beyond, Energy Environ. Mater. 4 (2021) 363–391.
[14] J. Prakash, H.C. Swart, G. Zhang, S. Sun, Emerging applications of atomic layer deposition for the rational design of novel nanostructures for surface-enhanced Raman scattering, J. Mater. Chem. C 7 (2019) 1447–1471.
[15] E.V. Formo, S.M. Mahurin, S. Dai, Robust SERS Substrates Generated by Coupling a Bottom-Up Approach and Atomic Layer Deposition, ACS Appl. Mater. Interfaces 2 (2010) 1987–1991.
[16] J.F. John, S. Mahurin, S. Dai, M.J. Sepaniak, Use of atomic layer deposition to improve the stability of silver substrates for in situ, high-temperature SERS measurements, J. Raman Spectrosc. 41 (2010) 4–11.
[17] L. Ma, Y. Huang, M. Hou, Z. Xie, Z. Zhang, Silver Nanorods Wrapped with Ultrathin Al_2O_3 Layers Exhibiting Excellent SERS Sensitivity and Outstanding SERS Stability, Sci. Rep. 5 (2015) 12890.
[18] L. Ma, Y. Huang, M. Hou, Z. Xie, Z. Zhang, Ag Nanorods Coated with Ultrathin TiO_2 Shells as Stable and Recyclable SERS Substrates, Sci. Rep. 5 (2015) 15442.
[19] S.S. Masango, R.A. Hackler, N. Large, A.-I. Henry, M.O. McAnally, G.C. Schatz, P. C. Stair, R.P. Van Duyne, High-resolution distance dependence study of surface-enhanced Raman scattering enabled by atomic layer deposition, Nano Lett. 16 (2016) 4251–4259.
[20] Y.-Q. Cao, K. Qin, L. Zhu, X. Qian, X.-J. Zhang, D. Wu, A.-D. Li, Atomic-Layer-Deposition Assisted Formation of Wafer-Scale Double-Layer Metal Nanoparticles with Tunable Nanogap for Surface-Enhanced Raman Scattering, Sci. Rep. 7 (2017) 5161.
[21] L. Lin, Q. Zhang, X. Li, M. Qiu, X. Jiang, W. Jin, H. Gu, D.Y. Lei, J. Ye, Electron Transport Across Plasmonic Molecular Nanogaps Interrogated with Surface-Enhanced Raman Scattering, ACS Nano 12 (2018) 6492–6503.
[22] K. Chen, X. Zhang, Y. Zhang, D.Y. Lei, H. Li, T. Williams, D.R. MacFarlane, Highly Ordered Ag/Cu Hybrid Nanostructure Arrays for Ultrasensitive Surface-Enhanced Raman Spectroscopy, Adv. Mater. Interfaces 3 (2016) 1600115.
[23] H. Duan, A.I. Fernández-Domínguez, M. Bosman, S.A. Maier, J.K.W. Yang, Nanoplasmonics: Classical down to the Nanometer Scale, Nano Lett. 12 (2012) 1683–1689.
[24] A. Cui, Z. Liu, H. Dong, Y. Wang, Y. Zhen, W. Li, J. Li, C. Gu, W. Hu, Single Grain Boundary Break Junction for Suspended Nanogap Electrodes with Gapwidth Down to 1–2 nm by Focused Ion Beam Milling, Adv. Mater. 27 (2015) 3002–3006.
[25] S.H. Park, J.G. Son, T.G. Lee, H.M. Park, J.o. Song, One-step large-scale synthesis of micrometer-sized silver nanosheets by a template-free electrochemical method, Nanoscale Res. Lett. 8 (2013) 248.
[26] J.-J. Zhu, X.-H. Liao, X.-N. Zhao, H.-Y. Chen, Preparation of silver nanorods by electrochemical methods, Mater. Lett. 49 (2001) 91–95.
[27] J. Choi, G. Sauer, K. Nielsch, R.B. Wehrspohn, U. Gösele, Hexagonally Arranged Monodisperse Silver Nanowires with Adjustable Diameter and High Aspect Ratio, Chem. Mater. 15 (2003) 776–779.
[28] B. Zhao, Y. Lu, C. Zhang, Y. Fu, S. Moeendarbari, S.R. Shelke, Y. Liu, Y. Hao, Silver dendrites decorated filter membrane as highly sensitive and reproducible three dimensional surface enhanced Raman scattering substrates, Appl. Surf. Sci. 387 (2016) 431–436.
[29] H.-X. Gu, L. Xue, Y.-F. Zhang, D.-W. Li, Y.-T. Long, Facile fabrication of a silver dendrite-integrated chip for surface-enhanced Raman scattering, ACS Appl. Mater. Interfaces 7 (2015) 2931–2936.
[30] M.U. Amin, L. Zhang, R. Hao, D. Zhang, H. You, J. Fang, Electrochemical growth of dendritic silver nanostructures as facile SERS substrates, CrystEngComm 23 (2021) 694–699.
[31] Z. Cheng, Y. Qiu, Z. Li, D. Yang, S. Ding, G. Cheng, Z. Hao, Q. Wang, Fabrication of silver dendrite fractal structures for enhanced second harmonic generation and surface-enhanced Raman scattering, Optical Mater. Express 9 (2019) 860.
[32] X.D. Zhou, X.H. Xiao, J.X. Xu, G.X. Cai, F. Ren, C.Z. Jiang, Mechanism of the enhancement and quenching of ZnO photoluminescence by ZnO-Ag coupling, EPL 93 (2011) 57009.
[33] M. Rahamim, H. Cohen, E. Edri, Chemistry and Charge Trapping at the Interface of Silver and Ultrathin Layers of Zinc Oxide, ACS Appl. Mater. Interfaces 13 (2021) 49423–49432.
[34] K. Sivashanmugan, J.-D. Liao, B.H. Liu, C.-K. Yao, S.-C. Luo, Ag nanoclusters on ZnO nanodome array as hybrid SERS-active substrate for trace detection of malachite green, Sensors Actuators B-Chem. 207 (2015) 430–436.
[35] P.B. Johnson, R.-W. Christy, Optical constants of the noble metals, Phys. Rev. B 6 (1972) 4370.
[36] I. Bodurov, I. Vlaeva, A. Viraneva, T. Yovcheva, S. Sainov, Modified design of a laser refractometer, Nanosci. Nanotechnol 16 (2016) 31–33.
[37] S. Chervinskii, A. Matikainen, A. Dergachev, A.A. Lipovskii, S. Honkanen, Out-diffused silver island films for surface-enhanced Raman scattering protected with TiO2 films using atomic layer deposition, Nanoscale Res. Lett. 9 (2014) 398.
[38] J. Lv, F. Lai, L. Lin, Y. Lin, Z. Huang, R. Chen, Thermal stability of Ag films in air prepared by thermal evaporation, Appl. Surf. Sci. 253 (2007) 7036–7040.
[39] E.C. Le Ru, E. Blackie, M. Meyer, P.G. Etchegoin, Surface Enhanced Raman Scattering Enhancement Factors: A Comprehensive Study, J. Phys. Chem. C 111 (2007) 13794–13803.
[40] W.A. Tegegne, W.-N. Su, A.B. Beyene, W.-H. Huang, M.-C. Tsai, B.-J. Hwang, Flexible hydrophobic filter paper-based SERS substrate using silver nanocubes for sensitive and rapid detection of adenine, Microchem. J. 168 (2021), 106349.